

Received October 2, 2019, accepted October 20, 2019, date of publication October 24, 2019, date of current version November 6, 2019.

Digital Object Identifier 10.1109/ACCESS.2019.2949252

Reduced Preisach Model: Beyond Discrete Empirical Interpolation Method

DAN WANG¹, YAoyao WANG^{1,2}, (Member, IEEE), YONGHUA LU¹, BAI CHEN¹, LINXIANG WANG², AND HONGTAO WU¹

¹National Key Laboratory of Science and Technology on Helicopter Transmission, Nanjing University of Aeronautics and Astronautics, Nanjing 210016, China

²State Key Laboratory of Fluid Power and Mechatronic Systems, Zhejiang University, Hangzhou 310029, China

Corresponding authors: Dan Wang (wangdan_053@nuaa.edu.cn) and Linxiang Wang (wanglx236@zju.edu.cn)

This work was supported in part by the National Natural Science Foundation of China under Grant 51575478, Grant 51975277, and Grant 51575277.

ABSTRACT The Preisach model, which is formulated as a weighted superposition of hysteresis kernels, has been widely used for hysteresis modeling, especially in smart-material-based actuators. However, in the classical Preisach model, a trade-off is always required between the model accuracy and the number of the hysteresis kernels. To deal with this problem, a model order reduction technique based on the discrete empirical interpolation method (DEIM) has recently been proposed. The method can largely reduce the number of the hysteresis kernels while barely losing the model accuracy. It is noted that the kernel weight in the reduced DEIM-based model can be both positive and negative, which means that the monotonicity of the Preisach model could be lost. The monotonicity is a very important property especially when constructing the inverse Preisach model. Furthermore, the loss of the monotonicity can also deteriorate the model predictability. In the current paper, a modification strategy is proposed. In the modified reduced Preisach model, the DEIM is only employed to select the dominant hysteresis kernels while the corresponding weights of the selected hysteresis kernels are re-identified by solving a constraint optimization problem. Systematic simulation studies and experimental validation are carried out to demonstrate the effectiveness of the proposed strategy.

INDEX TERMS Discrete empirical interpolation method (DEIM), hysteresis nonlinearity, monotonicity, reduced Preisach model, smart-material-based actuator.

I. INTRODUCTION

Due to their intrinsic multi-physics coupling effects and excellent properties, smart materials and structures have been widely employed for engineering applications, such as different smart-material-based actuators, sensors, energy harvesters and vibration dampers [1]–[8]. However, severe hysteresis nonlinearity is a common phenomenon present in the input-output response of these smart-material-based devices. The hysteresis nonlinearity can significantly affect the device performance and may even induce oscillations and instabilities [9], [10]. To compensate the negative influence of the hysteresis nonlinearity, and to analyze, control as well as optimize these smart-material-based devices, a hysteresis model should be developed at first [11]–[13]. Among the existing hysteresis models, the Preisach model has received

considerable attention, because it can capture the basic features of the hysteresis phenomenon in a conceptually simple and mathematically elegant manner. The Preisach model has been successfully used for describing hysteresis nonlinearity in many different smart materials and structures, especially in various smart-material-based actuators, such as piezoelectric, magnetostrictive and shape memory alloy actuators [14]–[18].

The Preisach model was firstly proposed by a German physicist Preisach in 1935. The original physics-based model was then extended by a Russian mathematician Krasnosel'skii, who separated the physical meaning from the original Preisach model and reformulated it as a pure mathematical model. As a phenomenological model, the Preisach model can capture various types of hysteresis nonlinearity. The continuous Preisach model is formulated as a double integral with respect to the two switching thresholds of the underlined hysteresis kernels. To facilitate the

The associate editor coordinating the review of this manuscript and approving it for publication was Yangmin Li¹.

implementation in real-world applications, the continuous form model needs to be discretized and the accuracy of the discrete Preisach model relies on the discretization level, which determines the number of the hysteresis kernels [19], [20]. A higher model accuracy requires a larger number of hysteresis kernels, which in turn leads to a heavier computational cost. To deal with this trade-off problem between the model accuracy and the number of the hysteresis kernels, different methods have been proposed in the literature. J. Zhang et al. proposed an optimal compression method based on the Kullback-Leibler (KL) divergence, which was utilized to measure the information loss in discretizing the Preisach model [21]. In the original work, the optimization was realized by an exhaustive search due to the particular setting of the Preisach plane. And an enhanced work based on dynamic programming was proposed for the generalized Prandtl–Ishlinskii model [22]. Recently, based on the discrete empirical interpolation method (DEIM), Z. Li et al. proposed a model order reduction strategy for the Preisach model [20]. The strategy can reduce the number of the hysteresis kernels to less than 5% of that of the original full-order model while barely losing the model accuracy [20], [23]. However, it is noted that the re-constructed weights corresponding to the selected dominant hysteresis kernels in the reduced Preisach model using the DEIM can be both positive and negative, which means that the monotonicity of the Preisach model could be lost.

Monotonicity is a vital important property associated with the Preisach model. Due to the absence of an analytical inversion, most existing inverse Preisach models, which are employed for feedforward control in smart-material-based actuators, are constructed numerically based on the monotonicity of the Preisach model [24]–[26]. Besides, the loss of the monotonicity may also deteriorate the model predictability. To preserve the monotonicity in the reduced model, a modified reduced Preisach model beyond the DEIM is proposed in the current paper. Firstly, the DEIM is employed to select the dominant hysteresis kernels. As for the weights corresponding to the selected dominant hysteresis kernels, instead of being constructed directly by the DEIM, they are re-identified by solving a constraint optimization problem. The nonnegative property of the kernel weights is guaranteed through the constraint adopted in the optimization process. The superiority of the proposed model will be demonstrated by a systematic comparison with the reduced model proposed by Z. Li et al.

The current paper is organized as follows. A brief introduction to the Preisach model is given in Section II, where a detailed discussion regarding the relationship between the monotonicity and the Preisach density function is carried out. Section III reviews the reduced Preisach model using the DEIM that was proposed by Z. Li et al. Besides, a detailed analysis of the problems associated with the reduced model using the DEIM and a modification strategy are also presented in Section III. Systematic simulation studies and experimental validation are respectively provided in

Section IV and Section V. Section VI summarizes the results of the current paper.

II. PREISACH MODEL

The classical Preisach model is formulated as a weighted superposition of hysteresis kernels with different switching thresholds:

$$y(t) = \iint_{\mathbf{T}} \mu(r, s) [\mathcal{R}_{s-r, s+r}(u)](t) dr ds, \quad (1)$$

where $u(t)$ denotes the input and $y(t)$ the output. $w(t) = [\mathcal{R}_{s-r, s+r}(u)](t)$ is a multivalued relay-type hysteresis kernel defined as:

$$w(t) = \begin{cases} +1, & \text{if } u(t) > s + r \\ -1, & \text{if } u(t) < s - r \\ w(t^-), & \text{if } s - r \leq u(t) \leq s + r, \end{cases} \quad (2)$$

where r and s are values that determine the switching thresholds, and $t^- = \lim_{\substack{\varrho \rightarrow 0, \varrho > 0}} (t - \varrho)$ represents the previous time. $\mu(r, s)$ is the density function of the Preisach model, which is defined on the Preisach plane $\mathbf{T} = \{(r, s) \in \mathbf{T} | r - \Omega < s < -r + \Omega, r \geq 0\}$ with a constant $\Omega > 0$.

The output evolution of the Preisach model is well understood via the Preisach plane. At each time t , the Preisach plane \mathbf{T} consists of the subsets, $\mathbf{T}_+(t)$ and $\mathbf{T}_-(t)$, where $\mathbf{T}_{\pm}(t) = \{(r, s) \in \mathbf{T}_{\pm} | (r, s) \in \mathbf{T}, \mathcal{R}_{s-r, s+r} = \pm 1\}$. Suppose that the input is increased from the negative limit $-\Omega$, where all the hysteresis kernels on the Preisach plane retain output -1 , monotonically to a value u_1 . The hysteresis kernels $\mathcal{R}_{s-r, s+r}$ with $s + r < u_1$ switch from -1 to $+1$, while those with $s + r > u_1$ retain output -1 , as illustrated in Fig. 1(a). If the input is then decreased monotonically from u_1 to u_2 , the hysteresis kernels with $s - r > u_2$ switches back from $+1$ to -1 , as shown in Fig. 1(b). A staircase-like curve that separates the region \mathbf{T}_+ from \mathbf{T}_- can be obtained with a piecewise-monotone input. As illustrated in Fig. 1(c), if the input takes a small variation $+\Delta u_1$ (or $-\Delta u_2$), the output variation can be expressed as: $+2 \iint_{\Delta \mathbf{T}_1} \mu(r, s)$ (or $-2 \iint_{\Delta \mathbf{T}_2} \mu(r, s)$). It is noted that the monotonicity of the Preisach model is determined by the signs of the integration of the density function $\mu(r, s)$ on the small incremental regions. With a nonnegative $\mu(r, s)$, the integration is always non-negative and the monotonicity of the model is automatically guaranteed. On the other hand, the monotonicity could be lost when the sign of the density function is indetermined.

In (1), the output of the Preisach model is expressed as a double integral with respect to r and s . To implement it in real-world applications, the double integral needs to be approximated through a numerical cubature technique. Generally, a discrete Preisach model can be formulated as:

$$y(t) = \sum \sum \mu_{ij} [\mathcal{R}_{ij}(u)](t) r_i s_j, \quad (3)$$

where μ_{ij} and $[\mathcal{R}_{ij}(u)](t)$ are respectively the values of $\mu(r, s)$ and $[\mathcal{R}_{s-r, s+r}(u)](t)$ at the discretization points, and r_i and s_j denote the weights of numerical integration.

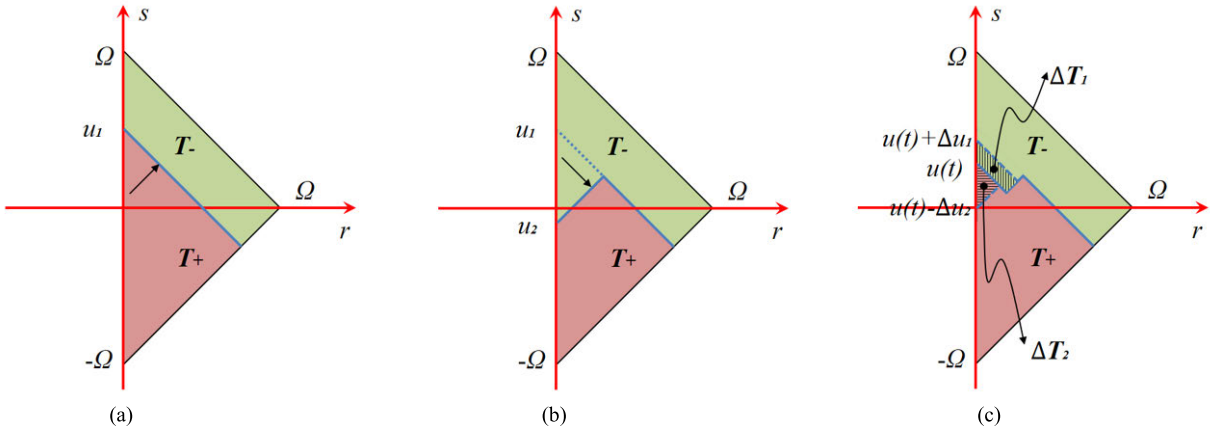


FIGURE 1. Illustration of the output evolution of the Preisach model via the Preisach plane. (a) The input monotonically increases from the negative limit to u_1 . (b) The input monotonically decreases from u_1 to u_2 . (c) The input takes small variations at $u(t)$.

Here, the Preisach plane is evenly discretized into L intervals along the $s + r$ and $s - r$ directions, which leads to a total discretization number $n = \frac{L(L+1)}{2}$. Employing the midpoint rule, the discrete Preisach model can be reconstructed as:

$$y(t) = \sum_{i=1}^L \sum_{j=1}^i \mu_{ij} [\mathcal{R}_{ij}(u)](t) \left(\frac{2\Omega^2}{L^2} \right). \quad (4)$$

To facilitate the identification of the Preisach density function $\mu(r, s)$ in real-world applications, the output of the discrete Preisach model is further reformulated as:

$$y(t) = \sum_{k=1}^n a_k w_k = \mathbf{a}^T \mathbf{w}, \quad (5)$$

where $\mathbf{a} = [a_1, a_2, \dots, a_n]^T = \frac{2\Omega^2}{L^2} [\mu_{11}, \mu_{21}, \dots, \mu_{LL}]^T$ is the combined weight vector, which includes the influence of the weight $\frac{2\Omega^2}{L^2}$, and $\mathbf{w} = [w_1, w_2, \dots, w_n]^T = [\mathcal{R}_{11}, \mathcal{R}_{21}, \dots, \mathcal{R}_{LL}]^T$ is the output vector of the hysteresis kernels at the corresponding discretization points.

III. REDUCED PREISACH MODEL

In the above discrete Preisach model employing numerical technique with evenly-distributed discretization points, the model prediction accuracy depends on the total discretization number n , namely, the total number of the hysteresis kernels. Only a large enough n can guarantee a sufficient model accuracy. However, on the other hand, a larger n also means a heavier computational cost. A trade-off needs to be made between the discretization number n and the model accuracy. As mentioned above, a reduced Preisach model based on the DEIM was proposed by Z. Li et al. to deal with this trade-off problem. m ($m \ll n$) dominant discretization points are selected from the original n points and the corresponding weights are constructed through the DEIM. Compared with the discrete Preisach model with m evenly-distributed discretization points, the proposed model can predict the nonlinear hysteresis more smoothly and accurately. In the following subsection, the method will be briefly reviewed at first.

A. REDUCED MODEL USING THE DEIM (RM-DEIM)

The DEIM is one of the most effective model order reduction techniques, and was originally developed to solve complex large-scale ordinary differential equation systems [27], [28]. DEIM approximates a nonlinear function by constructing a subspace through singular value decomposition (SVD) on a snapshot matrix of the nonlinear function and selecting interpolation indices through a recursive interpolation-based projection process. Due to its excellent performance, the DEIM has already been employed for model order reduction in numerous applications [29]–[31].

To employ the DEIM for model order reduction in the classical Preisach model, (5) is firstly reformulated as:

$$y(t) = [1, 1, \dots, 1] \cdot \mathbf{f}(t) = [1, 1, \dots, 1] \cdot \begin{bmatrix} a_1 w_1(t) \\ a_2 w_2(t) \\ \vdots \\ a_n w_n(t) \end{bmatrix}, \quad (6)$$

where the nonlinear vector function $\mathbf{f}(t) \in \mathbb{R}^{n \times 1}$ will be approximated by the DEIM. DEIM constructs an interpolation approximation function $\hat{\mathbf{f}}(t) \in \mathbb{R}^{n \times 1}$ of the original function by projecting it onto an m dimensional subspace as:

$$\mathbf{f}(t) \approx \mathbf{U}_m \mathbf{c}(t) = \hat{\mathbf{f}}(t), \quad (7)$$

where $\mathbf{U}_m = [\mathbf{u}_1, \mathbf{u}_2, \dots, \mathbf{u}_m] \in \mathbb{R}^{n \times m}$ is the m dimensional projection basis matrix and $\mathbf{c}(t) \in \mathbb{R}^{m \times 1}$ the interpolation coefficient vector.

The projection basis matrix \mathbf{U}_m is obtained through SVD on a snapshot matrix of $\mathbf{f}(t)$. The snapshot matrix can be constructed as:

$$\mathbf{Y} = \begin{bmatrix} a_1 w_1[u](t_1) & a_1 w_1[u](t_2) & \dots & a_1 w_1[u](t_M) \\ a_2 w_2[u](t_1) & a_2 w_2[u](t_2) & \dots & a_2 w_2[u](t_M) \\ \vdots & \vdots & \ddots & \vdots \\ a_n w_n[u](t_1) & a_n w_n[u](t_2) & \dots & a_n w_n[u](t_M) \end{bmatrix}, \quad (8)$$

TABLE 1. Algorithm [27].

Input: $\mathbf{U}_m = [\mathbf{u}_1, \mathbf{u}_2, \dots, \mathbf{u}_m] \in \mathbb{R}^{n \times m}$
Output: $\mathbf{P} \in \mathbb{R}^{n \times m}, \boldsymbol{\xi} = [\xi_1, \xi_2, \dots, \xi_m]^T \in \mathbb{R}^{m \times 1}$
$[\ \rho\ , \xi_1] = \max\{\ \mathbf{u}_1\ \}$
$\mathbf{U}_l = [\mathbf{u}_1], \mathbf{P} = [\mathbf{e}_{\xi_1}], \boldsymbol{\xi} = [\xi_1]$
for $l = 2$ to m do
Solve $(\mathbf{P}^T \mathbf{U}_l) \mathbf{c}_l = \mathbf{P}^T \mathbf{u}_l$ for \mathbf{c}_l
$\mathbf{r} = \mathbf{u}_l - \mathbf{U}_l \mathbf{c}_l$
$[\ \rho\ , \xi_l] = \max\{\ \mathbf{r}\ \}$
$\mathbf{U}_l \leftarrow [\mathbf{U}_l, \mathbf{u}_l], \mathbf{P} = [\mathbf{P}, \mathbf{e}_{\xi_l}], \boldsymbol{\xi} = [\boldsymbol{\xi}^T, \xi_l]^T$
end for

where $u(t_1), u(t_2), \dots, u(t_M)$ is an excitation signal sequence. By applying SVD on the matrix \mathbf{Y} , one obtains:

$$\mathbf{Y} = \mathbf{U}\mathbf{S}\mathbf{V}^T, \tag{9}$$

where $\mathbf{U} \in \mathbb{R}^{n \times n}$ contains the left singular vectors, $\mathbf{S} \in \mathbb{R}^{n \times M}$ is a diagonal matrix with the singular values listed on the diagonal in a descending order, and $\mathbf{V} \in \mathbb{R}^{M \times M}$ contains the right singular vectors. The first m dominant singular vectors in matrix \mathbf{U} make up the projection basis matrix \mathbf{U}_m . Clearly, the empirically derived projection basis through SVD on the snapshot matrix \mathbf{Y} depends on the selection of the excitation signal sequence, which needs to be sufficiently abundant.

To give a proper expression for the coefficient vector $\mathbf{c}(t)$, a matrix $\mathbf{P} = [\mathbf{e}_{\xi_1}, \mathbf{e}_{\xi_2}, \dots, \mathbf{e}_{\xi_m}] \in \mathbb{R}^{n \times m}$ is firstly derived from a recursive algorithm as shown in Table 1. \mathbf{e}_{ξ_l} is the ξ_l th column of the identity matrix $\mathbf{E} \in \mathbb{R}^{n \times n}$. At each iteration, the algorithm selects the index ξ_l corresponding to the entry of the residual vector $\mathbf{r} = \mathbf{u}_l - \mathbf{U}_l \mathbf{c}_l$ with the largest magnitude to limit growth of the error bound [27]. At the l th iteration, all the ξ_i th ($i = 1, 2, \dots, l - 1$) entry of the residual vector \mathbf{r} are guaranteed to be 0. For more details about the algorithm, [27] can be referred to. Multiplying \mathbf{P}^T on both sides of (7) leads to:

$$\mathbf{P}^T \mathbf{f}(t) \approx \mathbf{P}^T \mathbf{U}_m \mathbf{c}(t). \tag{10}$$

As $\mathbf{P}^T \mathbf{U}_m$ is nonsingular, which has been proved in [27], $\mathbf{c}(t)$ is deduced as:

$$\mathbf{c}(t) \approx (\mathbf{P}^T \mathbf{U}_m)^{-1} \mathbf{P}^T \mathbf{f}(t), \tag{11}$$

where the last two terms $\mathbf{P}^T \mathbf{f}(t) = \mathbf{f}_m(t) = [a_{\xi_1} w_{\xi_1}(t), a_{\xi_2} w_{\xi_2}(t), \dots, a_{\xi_m} w_{\xi_m}(t)]^T$ together represent the selected m elements from $\mathbf{f}(t)$. In this way, the interpolation approximation function $\hat{\mathbf{f}}(t)$ can be formulated as:

$$\hat{\mathbf{f}}(t) \approx \mathbf{U}_m (\mathbf{P}^T \mathbf{U}_m)^{-1} \mathbf{f}_m(t), \tag{12}$$

where only the selected m elements from the original nonlinear vector function $\mathbf{f}(t)$ are needed. Given that the output of the discrete Preisach model is exactly the sum of all the elements in $\mathbf{f}(t)$ or $\hat{\mathbf{f}}(t)$, it is obvious that in the RM-DEIM only m hysteresis kernels corresponding to the selected m elements are effective. Therefore, the total kernel number

employed in the reduced Preisach model has been reduced from n to m . Assuming

$$\mathbf{U}_m (\mathbf{P}^T \mathbf{U}_m)^{-1} = \begin{bmatrix} \lambda_{11} & \lambda_{12} & \dots & \lambda_{1m} \\ \lambda_{21} & \lambda_{22} & \dots & \lambda_{2m} \\ \vdots & \vdots & \ddots & \vdots \\ \lambda_{n1} & \lambda_{n2} & \dots & \lambda_{nm} \end{bmatrix}, \tag{13}$$

the output of the RM-DEIM can be expressed as:

$$\begin{aligned} \hat{\mathbf{y}}(t) &= [1, 1, \dots, 1] \cdot \hat{\mathbf{f}}(t) \\ &= \sum_{j=1}^m \sum_{i=1}^n \lambda_{ij} a_{\xi_j} w_{\xi_j}(t) = \sum_{j=1}^m \alpha_{\xi_j} w_{\xi_j}(t), \end{aligned} \tag{14}$$

where $\alpha_{\xi_j} = \sum_{i=1}^n \lambda_{ij} a_{\xi_j}$ denotes the corresponding weight for the selected hysteresis kernel $w_{\xi_j}(t)$. For more details regarding the RM-DEIM, the interested readers can consult [20].

B. PROBLEMS WITH RM-DEIM AND A MODIFICATION STRATEGY

The RM-DEIM reviewed above can predict the nonlinear hysteresis with a largely reduced computational cost while barely losing the model accuracy, which has been illustrated through systematic simulation studies and experimental validation in [20]. However, in the RM-DEIM, the weight $\alpha_{\xi_j} = \sum_{i=1}^n \lambda_{ij} a_{\xi_j}$ calculated from the interpolation projection process can be negative, which means that the monotonicity of the original full-order Preisach model (FM) could be lost. To give an illustration, a numerical simulation is carried out. As in [20], a factorized-Lorentzian density function:

$$\mu(r, s) = \Psi \left[1 + \left(\frac{r - \delta}{\sigma \delta} \right)^2 \right]^{-1} \left[1 + \left(\frac{s + \delta}{\sigma \delta} \right)^2 \right]^{-1}, \tag{15}$$

is employed for constructing the FM. Besides, $\Psi = 2$, $\delta = 1$ and $\sigma = 1$ are respectively adopted. The bound Ω is kept as 4 and the total discretization number n is selected as $\frac{161 \times (161 + 1)}{2} = 13041$. To construct the RM-DEIM, $m = 600$ dominant hysteresis kernels are used. Additional details about the simulation will be provided in the next section. As shown in Fig. 2(a), the weight $\alpha_{\xi_j} = \sum_{i=1}^n \lambda_{ij} a_{\xi_j}$ calculated from the DEIM can be both negative and positive. As a result, it is noted from the zoomed-in plot of Fig. 2(b) that the monotonicity of the FM has been lost even though the general model accuracy is acceptable. Monotonicity is a very important property of the Preisach model, particularly when an inverse Preisach model needs to be numerically constructed for feedforward control design of smart-material-based actuators [24]–[26]. In addition, monotonicity can also enhance the model predictability and precision, which will be demonstrated in the following discussion.

To deal with the problem pointed out above, a modification strategy is proposed in this subsection. Firstly, m dominant hysteresis kernels are selected by the DEIM. However, in the modified model, the weight $\alpha_{\xi_j} = \sum_{i=1}^n \lambda_{ij} a_{\xi_j}$ calculated from the DEIM is not adopted. Instead, a constraint least

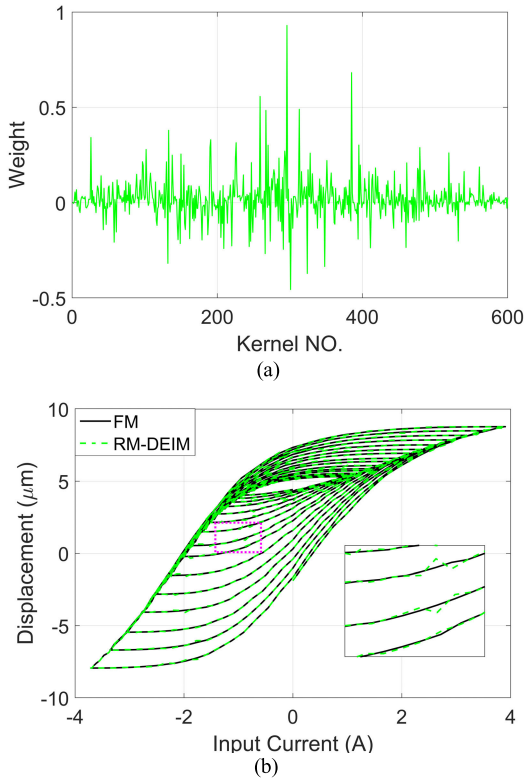


FIGURE 2. Illustration of the problems associated with the RM-DEIM. (a) Indetermined kernel weight. (b) Loss of monotonicity in the hysteresis curves.

square optimization problem is further solved to determine the new weight:

$$\min_{\alpha} \|W\alpha - y\|^2, \quad \text{s.t. } \alpha \geq 0. \quad (16)$$

Here

$$W = \begin{bmatrix} w_{\xi_1}[u](t_1) & w_{\xi_1}[u](t_2) & \cdots & w_{\xi_1}[u](t_M) \\ w_{\xi_2}[u](t_1) & w_{\xi_2}[u](t_2) & \cdots & w_{\xi_2}[u](t_M) \\ \vdots & \vdots & \ddots & \vdots \\ w_{\xi_m}[u](t_1) & w_{\xi_m}[u](t_2) & \cdots & w_{\xi_m}[u](t_M) \end{bmatrix}^T \quad (17)$$

denotes the response matrix of the selected m hysteresis kernels to the identification signal sequence $u(t_1), u(t_2), \dots, u(t_M)$, which is selected same to the excitation signal sequence that is used to construct the snapshot matrix Y . Further

$$\alpha = [\alpha_{\xi_1}, \alpha_{\xi_2}, \dots, \alpha_{\xi_m}]^T \quad (18)$$

gives the optimized weights for the selected hysteresis kernels, and

$$y = [y(t_1), y(t_2), \dots, y(t_M)]^T \quad (19)$$

is the output vector of the FM or real experimental data. In the proposed modification strategy, the nonnegative property of the weight vector α is guaranteed through the constraint

adopted in the optimization process. Therefore, the monotonicity of the Preisach hysteresis model is preserved. Furthermore, the lost information contained in the right singular vector matrix V in the SVD process is recovered through the constraint least square optimization process.

As a comparison, another model with weights optimized through a pure least square optimization algorithm without any constraint is proposed next. The corresponding optimization problem can be formulated as:

$$\min_{\alpha} \|W\alpha - y\|^2, \quad (20)$$

where W , α and y are the same as in (16). In the following section, the merits and drawbacks of the proposed modified model will be illustrated through a systematic comparison with the RM-DEIM, FM and above reference model. For convenience, the models with weights optimized through (16) and (20) are respectively denoted as RM-DEIM-M and RM-DEIM-R.

IV. SIMULATION STUDIES

To give a systematic comparison of the above three different reduced Preisach models, an FM needs to be constructed at first. To this end, a factorized-Lorentzian type density function as in (15) is employed. The model parameters are selected as: $\Psi = 2$, $\delta = 1$, $\sigma = 1$ and $\Omega = 4$. Besides, to discretize the Preisach plane T , a total discretization number $n = 13041$ is adopted. As for the construction of the three reduced models, a snapshot matrix Y is formulated by using a decreasing sinusoidal excitation signal $u_e(t) = 4e^{-0.1t} \sin(2\pi t)$. The total length of the signal and the sampling time are respectively taken as 15s and 0.01s, which means that $M = 1501$ sampling points are used. Afterwards, by applying SVD on the snapshot matrix Y and choosing an appropriate reduced order m , one obtains the projection basis matrix U_m . Further applying the algorithm as listed in Table 1 gives the indices of the selected m dominant hysteresis kernels. The corresponding weights of the selected m dominant hysteresis kernels for the three different reduced models are obtained respectively from (14), (16) and (20).

Fig. 3 gives a detailed comparison of the modeling performance of the three reduced Preisach models when a reduced order $m = 600$ is used. As shown in Fig. 3(a), the optimized weights for RM-DEIM-M are all positive while the weights for RM-DEIM-R can be both positive and negative, which agrees with the constraints employed in the optimization processes. It is noted from Fig. 3(b) that the model accuracy of all these three reduced models is generally acceptable.

However, from the zoomed-in plot in Fig. 3(b), RM-DEIM-M and RM-DEIM-R can follow the input-output response of the FM more precisely, without any local up-and-down variations. Besides, Fig. 3(c) shows a detailed comparison of the modeling errors of the three different reduced models. The modeling error is defined as:

$$Error(t) = \frac{y_{rm}(t) - y_{fm}(t)}{\max(y_{fm}) - \min(y_{fm})}, \quad (21)$$

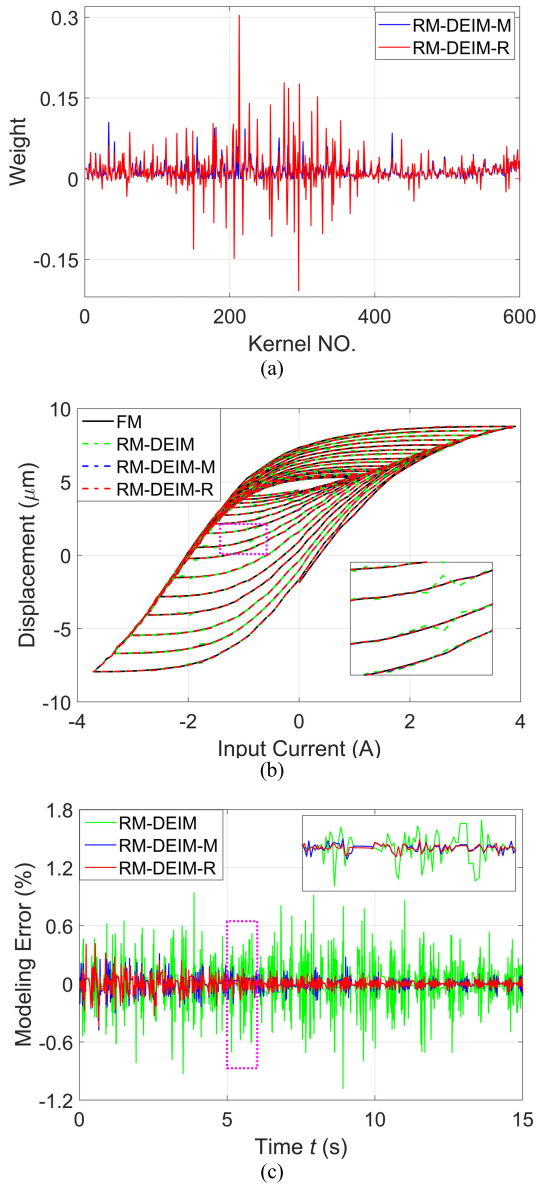


FIGURE 3. Comparison of the modeling performance of the three reduced Preisach models when $m = 600$. (a) Re-identified kernel weights of RM-DEIM-M and RM-DEIM-R. (b) Input-output response. (c) Detailed modeling error.

where $y_{rm}(t)$ and $y_{fm}(t)$ denote the output of the reduced model and FM respectively, while $\max(\cdot)$ and $\min(\cdot)$ represent maximum and minimum functions. Compared with the RM-DEIM, the modeling errors of RM-DEIM-M and RM-DEIM-R have been largely reduced. It is also noted from the zoomed-in plot of Fig. 3(c) that, to some extent, the modeling errors of the two new models coincide with each other, which would be different when $m = 1000$ was used. Detailed explanations for this difference will be given in the following discussion.

To investigate the influence of the reduced order m on the modeling performance of the three different reduced Preisach models, numerical simulations with various reduced order m (400, 500, 600, 800 and 1000) are carried out. The average

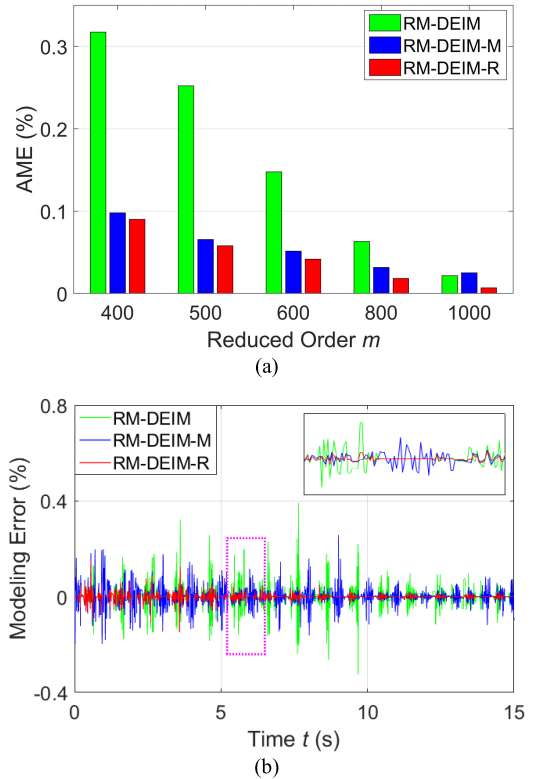


FIGURE 4. Comparison of the modeling performance with different m . (a) Average modeling error (AME). (b) Detained modeling error when $m = 1000$.

modeling errors (AMEs) of the three reduced models with different reduced order m are demonstrated by a bar chart in Fig. 4(a). Generally, two observations can be made: 1) the AMEs of all three reduced models decrease as the reduced order m increases; 2) with a constant m , the modeling error of the RM-DEIM is always the largest while for RM-DEIM-R it is the smallest. It is noted from Fig. 4(a) that the modeling errors of the two new models are less than half of that of the RM-DEIM when $m = 400$ is used. However, with a larger m , the modification effect of RM-DEIM-M is not that obvious, and when $m = 1000$ is used, the performance is even worse than that of the RM-DEIM. Besides, Fig. 4(b) shows a detailed comparison of the modeling errors of the three different reduced models with $m = 1000$. As mentioned above, it is noted from the zoomed-in plot in Fig. 4(b) that the modeling error of RM-DEIM-M cannot follow the trend of RM-DEIM-R any more as in Fig. 3(c). All these observations can be ascribed to the balance of two distinct effects. On the one hand, the weight re-identification process in RM-DEIM-M and RM-DEIM-R can recover the lost information contained in the right singular vector matrix V , which will improve the model accuracy. On the other hand, the imposed nonnegative constraint in RM-DEIM-M will deteriorate the accuracy. With a large reduced order m , the influence of the nonnegative constraint becomes prominent, which is verified by the non-congruent modeling errors between the two new models. This results in a poor modeling

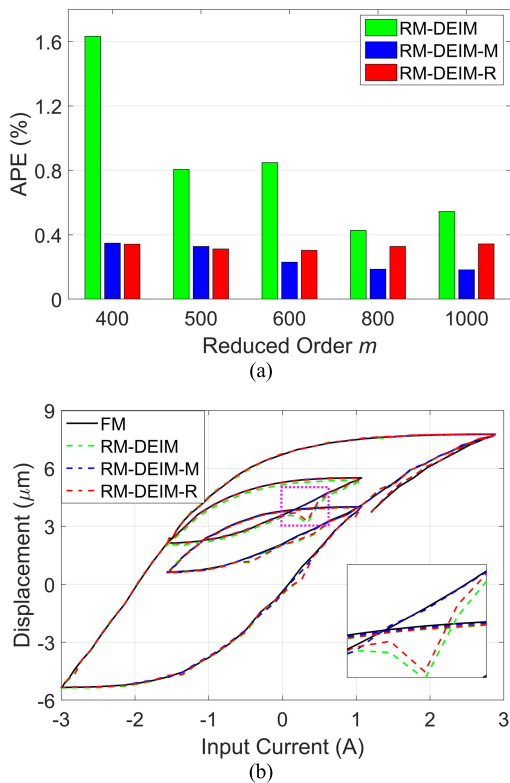


FIGURE 5. Comparison of the prediction ability with different m . (a) Average prediction error (APE). (b) Input-output response when $m = 1000$.

performance of RM-DEIM-M. However, when a small m is selected, the influence of the nonnegative constraint is not that obvious, and the performance of the two new models almost coincides with each other. They are much better than that of the RM-DEIM. In a word, the AME of RM-DEIM-R is closer to that of RM-DEIM-M when a smaller m is used, while it is closer to that of the RM-DEIM with a larger m .

To further compare the prediction ability of the three reduced models, a different signal $u_t(t) = 1.8\sin((10\pi/2.8571)t) + 1.2\sin(\pi t + \pi/2)$ is fed into the FM and three reduced models. This test signal has been carefully designed, which can verify the congruent property of the reduced Preisach models. The length of the signal and sampling time are respectively taken as 2s and 0.01s. Fig. 5(a) shows the average prediction errors (APEs) of the three different reduced models with different m . Generally, the APEs of the three reduced models decrease as the reduced order m increases. However, this tendency keeps much better for RM-DEIM-M than for the other two reduced models. In addition, it is also noted that RM-DEIM-M always retains the best prediction ability among these three reduced models, which is different from the case regarding AMEs as demonstrated in Fig. 4(a), particularly for $m = 1000$. These observations can be explained by the fact that the monotonicity of the original Preisach model is well preserved in RM-DEIM-M. Fig. 5(b) gives a comparison of the hysteresis curves of the three reduced models along with the input-output response

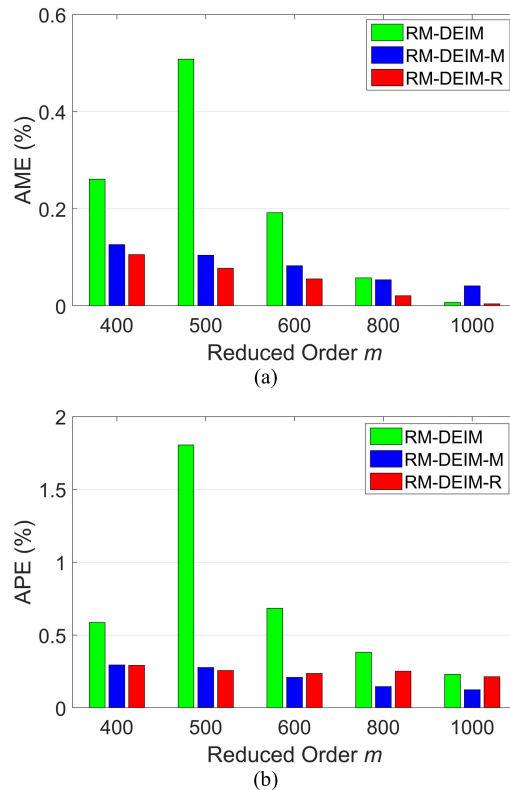


FIGURE 6. Comparison of the working performance with a Gauss I density function. (a) Average modeling error (AME). (b) Average prediction error (APE).

of the FM when $m = 1000$. It is noted that within the boxed area an obvious up-and-down variation exists both for the RM-DEIM and RM-DEIM-R. However, good monotonicity of RM-DEIM-M keeps its response on track with the FM. Monotonicity increases the model predictability and precision!

As in [20], in addition to the factorized-Lorentzian function, two Gauss-type density functions:

Gauss I

$$\mu(r, s) = \Psi e^{-\left(\frac{r-s}{2} - \delta\right)^2 / (2\sigma^2\delta^2)} e^{-\left(\frac{r+s}{2}\right)^2 / (2\sigma^2\delta^2)}, \quad (22)$$

and Gauss II

$$\mu(r, s) = \Psi \frac{1}{2\pi\sigma\zeta} e^{-\frac{(r-\delta)^2}{2\sigma^2} - \frac{s^2}{\zeta^2}}, \quad (23)$$

are further employed to investigate the influence of the density function on the performance of the three different reduced models. For Gauss I, the parameters are selected as: $\Psi = 2$, $\delta = 0.4$ and $\sigma = 1.5$; and for Gauss II, the parameters are as: $\Psi = 2$, $\sigma = 2$ and $\zeta = 2$. Fig. 6(a) gives a bar chart of the AMEs of the three reduced models with different reduced order m when (22) is employed for model construction. The corresponding bar chart of the APEs is demonstrated in Fig. 6(b). Similar observations can be obtained as for the case with factorized-Lorentzian density function. However, it is noted that the AME and APE of the RM-DEIM both retain an abnormal increase when $m = 500$. This abnormal error

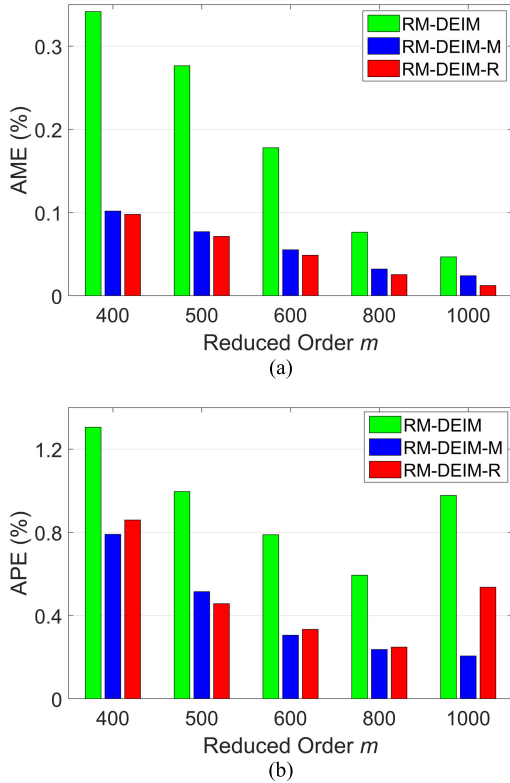


FIGURE 7. Comparison of the working performance with a Gauss II density function. (a). Average modeling error (AME). (b). Average prediction error (APE).

increase can be ascribed to the absence of the monotonicity in the RM-DEIM. Besides, the corresponding results associated with Gauss II density function are given in Fig. 7(a)-(b). It is noted that the APEs of both the RM-DEIM and RM-DEIM-R retain an abnormal increase when $m = 1000$, which could be ascribed to the loss of monotonicity. Small up-and-down variations could be present in the input-output response similar to the case as demonstrated in Fig. 5(b) and will deteriorate the prediction ability. From the above systematic simulation studies, following conclusions can be made: 1) compared with the RM-DEIM, the modeling errors of the two new reduced models are significantly reduced (with a small m , the error is even less than half of that associated with the RM-DEIM); 2) due to the preserved monotonicity, the prediction ability of RM-DEIM-M is the best, even better than that of RM-DEIM-R; 3) due to the preserved monotonicity, both the AME and APE of RM-DEIM-M decrease strictly as the reduced order m increases.

V. EXPERIMENTAL VALIDATION

To further verify the above observations, the experimental data sets from [20] are employed in this section for model validation. The experimental data was obtained from a magnetostrictive actuator, which is a typical smart-material-based actuator. The principle diagram of the experimental platform is presented in Fig. 8, which consists of a magnetostrictive actuator, a power amplifier, a capacitive dis-

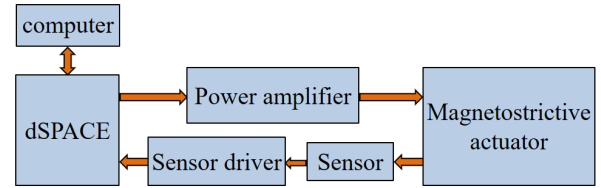


FIGURE 8. Principle diagram of the experimental platform.

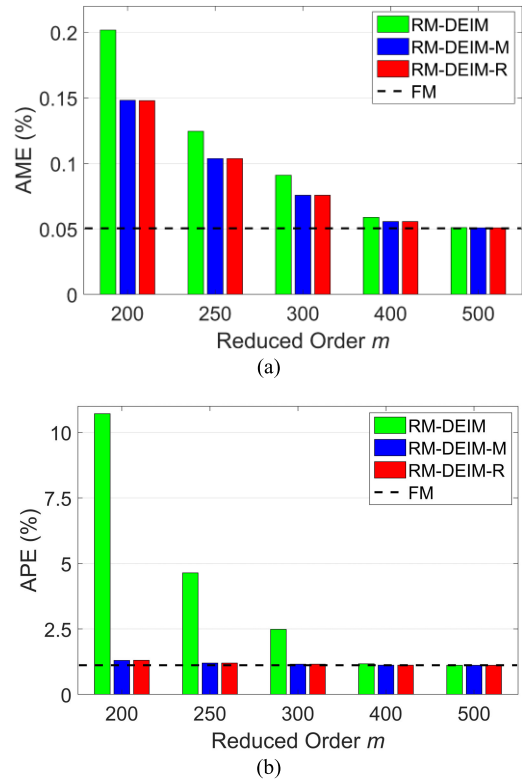


FIGURE 9. Experimental validation results I. (a) Average modeling error (AME). (b) Average prediction error (APE).

placement sensor, a sensor driver and a dSPACE control board. Following [20], an FM is constructed first as a reference. The experimental data corresponding to the decreasing sinusoidal signal $u_i(t) = 4.5\sin(2\pi t)e^{-0.2t}$ is adopted for identification of the density function $\mu(r, s)$. Instead of a specific form density function as given by (15), (22) or (23), a general form density function is employed for convenience, which can be easily identified through a nonnegative constraint least square optimization algorithm. For construction of the FM, a discretization number $n = \frac{181(181+1)}{2} = 16471$ and a bound constant $\Omega = 4.5$ are respectively used. With the FM constructed and the reduced order number m selected, the DEIM is further used to choose the m dominant hysteresis kernels. The same signal $u_i(t) = 4.5\sin(2\pi t)e^{-0.2t}$ is adopted as the excitation signal to construct the snapshot matrix Y . As for the weights corresponding to the m dominant hysteresis kernels, they can be obtained respectively from (14), (16) and (20).

Fig. 9(a) gives a bar chart of the AMEs of the three reduced models with different reduced order m . The black dashed line represents the modeling error of the FM. Generally, the mod-

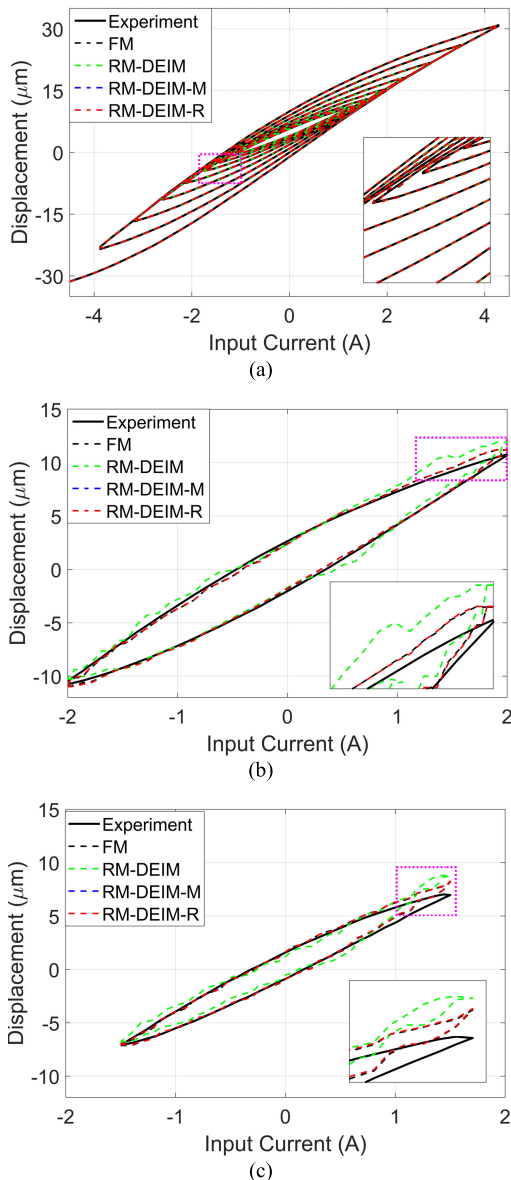


FIGURE 10. Experimental validation results II. (a) Input-output response with $m = 300$ when $u_i(t)$ is used as the input. (b) Input-output response with $m = 300$ when $u_{t1}(t)$ is used as the input. (c) Input-output response with $m = 300$ when $u_{t1}(t)$ is used as the input.

eling performance of both RM-DEIM-M and RM-DEIM-R is better than that of the RM-DEIM. It is also noted that the AMEs of the three reduced models converge to that of the FM when $m > 400$. The convergence is more rapid than that in the above simulation studies. This can be ascribed to the limited (not sufficiently abundant) information provided by the experimental data, which only needs to be described by a much more reduced-order model. As pointed out above, with a small reduced order m , the supplementary effect of the non-negative constraint is not that prominent and the optimized results of the two new reduced models almost coincide with each other. Therefore, the AMEs of the two new models are nearly equal.

Furthermore, the experimental data corresponding to a sinusoidal signal $u_{t1}(t) = 2\sin(2\pi t)$ and a triangular signal $u_{t2}(t)$ with period 1s and amplitude from -1.5 to 1.5 is employed to test the prediction abilities of the three reduced models. The bar chart of the APEs is demonstrated in Fig. 9(b). Due to the preserved monotonicity of RM-DEIM-M, its prediction error almost coincides with that of the FM, even when a very small reduced order $m = 200$ is used. As pointed out above, within the considered region, the working performance of RM-DEIM-R coincides with that of RM-DEIM-M, which gives it a much better result than that of the RM-DEIM. Besides, Fig. 10(a)-(c) show a detailed comparison of the input-output responses of these different hysteresis models and the experimental data when the identification signal $u_i(t)$ and test signals $u_{t1}(t)$ and $u_{t2}(t)$ are respectively employed as the input signal. The reduced order m is set as 300. The distinction between the hysteresis curves in Fig. 10(a) can be hardly noticed even from the zoomed-in plot. However, in Fig. 10(b)-(c), the predicted input-output response by the RM-DEIM is quite different from the experimental data, while the prediction errors of the two new models are coincided with that of the FM and is generally acceptable.

VI. CONCLUSION

In the current paper, a modified reduced Preisach model beyond DEIM, termed as RM-DEIM-M, has been proposed. In the modified model, the DEIM is employed first to select the dominant hysteresis kernels. Then, a constraint optimization problem is further solved to re-identify the corresponding weights of the selected hysteresis kernels. The monotonicity is well preserved in the modified model through the constraint adopted in the weight re-identification process. The superiority of the modification strategy has been illustrated through systematic simulation studies and experimental validation. The modeling error of the modified model can be reduced to less than half of that of the RM-DEIM when a small reduced order m is used. Besides, the model predictability has been largely improved due to the preserved monotonicity.

REFERENCES

- [1] Z. Deng, Q. Zhang, and M. J. Dapino, "Dynamic model for magnetostrictive systems with applications to damper design," *IEEE/ASME Trans. Mechatronics*, vol. 23, no. 4, pp. 1823–1831, Aug. 2018.
- [2] Z. Zhakypov, J.-L. Huang, and J. Paik, "A novel torsional shape memory alloy actuator: Modeling, characterization, and control," *IEEE Robot. Autom. Mag.*, vol. 23, no. 3, pp. 65–74, Sep. 2016.
- [3] L. Zhang, F. Ju, Y. Cao, Y. Wang, and B. Chen, "A tactile sensor for measuring hardness of soft tissue with applications to minimally invasive surgery," *Sens. Actuators A, Phys.*, vol. 266, pp. 197–204, Oct. 2017.
- [4] D. Wang, L. Wang, and R. Melnik, "Vibration energy harvesting based on stress-induced polarization switching: A phase field approach," *Smart Mater. Struct.*, vol. 16, no. 6, May 2017, Art. no. 065022.
- [5] D. Wang, H. Du, L. Wang, and R. Melnik, "A phase field approach for the fully coupled thermo-electro-mechanical dynamics of nanoscale ferroelectric actuators," *Smart Mater. Struct.*, vol. 27, no. 5, Apr. 2018, Art. no. 055012.

- [6] X. Rui, Z. Zeng, Y. Zhang, Y. Li, X. Huang, Y. Liu, and T. Xu, "An intelligent self-powered pipeline inner spherical detector with piezoelectric energy harvesting," *IEEE Access*, vol. 7, pp. 104621–104629, 2019.
- [7] T. Jin, Y. Peng, Z. Xing, and L. Lei, "A charge controller for synchronous linear operation of multiple piezoelectric actuators," *IEEE Access*, vol. 7, pp. 90741–90749, Jul. 2019.
- [8] J. Huang, L. Zou, P. Tian, Q. Zhang, Y. Wang, and J.-H. Zhang "A valveless piezoelectric micropump based on projection micro litho stereo exposure technology," *IEEE Access*, vol. 7, pp. 77340–77347, May 2019.
- [9] G.-Y. Gu, L.-M. Zhu, C.-Y. Su, H. Ding, and S. Fatikow, "Modeling and control of piezo-actuated nanopositioning stages: A survey," *IEEE Trans. Autom. Sci. Eng.*, vol. 13, no. 1, pp. 313–332, Jan. 2016.
- [10] A. G. Hatch, R. C. Smith, T. De, and M. V. Salapaka, "Construction and experimental implementation of a model-based inverse filter to attenuate hysteresis in ferroelectric transducers," *IEEE Trans. Control Syst. Technol.*, vol. 4, no. 6, pp. 1058–1069, Nov. 2006.
- [11] G.-Y. Gu, L.-M. Zhu, C.-Y. Su, and H. Ding, "Motion control of piezoelectric positioning stages: Modeling, controller design, and experimental evaluation," *IEEE/ASME Trans. Mechatronics*, vol. 18, no. 5, pp. 1459–1471, Oct. 2013.
- [12] G.-Y. Gu, L.-M. Zhu, and C.-Y. Su, "Modeling and compensation of asymmetric hysteresis nonlinearity for piezoceramic actuators with a modified Prandtl–Ishlinskii model," *IEEE Trans. Ind. Electron.*, vol. 61, no. 3, pp. 1583–1595, Mar. 2014.
- [13] G.-Y. Gu, M.-J. Yang, and L.-M. Zhu, "Real-time inverse hysteresis compensation of piezoelectric actuators with a modified Prandtl–Ishlinskii model," *Rev. Sci. Instrum.*, vol. 83, no. 6, Jun. 2012, Art. no. 065106.
- [14] G. Song, J. Zhao, X. Zhou, and J. A. De Abreu-Garcia, "Tracking control of a piezoceramic actuator with hysteresis compensation using inverse Preisach model," *IEEE/ASME Trans. Mechatronics*, vol. 10, no. 2, pp. 198–209, Apr. 2005.
- [15] H. Hu and R. Ben Mrad, "On the classical Preisach model for hysteresis in piezoceramic actuators," *Mechatronics*, vol. 13, no. 2, pp. 85–94, Apr. 2003.
- [16] Z. Li, C.-Y. Su, and T. Chai, "Compensation of hysteresis nonlinearity in magnetostrictive actuators with inverse multiplicative structure for Preisach model," *IEEE Trans. Autom. Sci. Eng.*, vol. 11, no. 2, pp. 613–619, Apr. 2014.
- [17] B.-J. Choi, Y.-J. Lee, and B.-Y. Choi, "Fast Preisach modeling method for shape memory alloy actuators using major hysteresis loops," *Smart Mater. Struct.*, vol. 13, no. 5, pp. 1069–1080, 2004.
- [18] S. Xiao and Y. Li, "Modeling and high dynamic compensating the rate-dependent hysteresis of piezoelectric actuators via a novel modified inverse Preisach model," *IEEE Trans. Control Syst. Technol.*, vol. 21, no. 5, pp. 1549–1557, Sep. 2013.
- [19] J. Å. Stakvik, M. R. P. Ragazzon, A. A. Eielsen, and J. T. Gravidahl, "On implementation of the Preisach model: Identification and inversion for hysteresis compensation," *Model., Identificat. Control*, vol. 36, no. 3, pp. 133–142, 2015.
- [20] Z. Li, J. Shan, and U. Gabbert, "Development of reduced Preisach model using discrete empirical interpolation method," *IEEE Trans. Ind. Electron.*, vol. 65, no. 10, pp. 8072–8079, Oct. 2018.
- [21] J. Zhang, E. Merced, N. Sepúlveda, and X. Tan, "Kullback-Leibler divergence-based optimal compression of Preisach operator in hysteresis modeling," in *Proc. Amer. Control Conf.*, Jun. 2013, pp. 89–94.
- [22] J. Zhang, E. Merced, N. Sepúlveda, and X. Tan, "Optimal compression of generalized Prandtl–Ishlinskii hysteresis models," *Automatica*, vol. 57, pp. 170–179, Jul. 2015.
- [23] Z. Li, J. Shan, and U. Gabbert, "Inverse compensator for a simplified discrete Preisach model using model-order reduction approach," *IEEE Trans. Ind. Electron.*, vol. 66, no. 8, pp. 6170–6178, Aug. 2019.
- [24] R. Venkataraman and P. S. Krishnaprasad, "Approximate inversion of hysteresis: Theory and numerical results," in *Proc. 39th IEEE Conf. Decis. Control*, Dec. 2000, pp. 4448–4454.
- [25] X. Tan and J. S. Baras, "Modeling and control of hysteresis in magnetostrictive actuators," *Automatica*, vol. 40, no. 9, pp. 1469–1480, 2004.
- [26] R. V. Iyer and X. Tan, "Control of hysteretic systems through inverse compensation," *IEEE Control Syst.*, vol. 29, no. 1, pp. 83–99, Feb. 2009.
- [27] S. Chaturantabud and D. C. Sorensen, "Nonlinear model reduction via discrete empirical interpolation," *SIAM J. Sci. Comput.*, vol. 32, no. 5, pp. 2737–2764, 2010.
- [28] S. Chaturantabud and D. C. Sorensen, "A state space error estimate for POD-DEIM nonlinear model reduction," *SIAM J. Numer. Anal.*, vol. 50, no. 1, pp. 46–63, 2012.
- [29] Z. Li, D. Danilov, M. C. F. Donkers, and H. J. Bergveld, "Model order reduction of Li-ion batteries via POD and DEIM," in *Proc. 35th Benelux Meeting Syst. Control*, Soesterberg, The Netherlands, 2016, p. 43.
- [30] A. Radermacher and S. Reese, "POD-based model reduction with empirical interpolation applied to nonlinear elasticity," *Int. J. Numer. Methods Eng.*, vol. 107, no. 6, pp. 477–495, Aug. 2016.
- [31] Y. Paquay, O. Brüls, and C. Geuzaine, "Nonlinear interpolation on manifold of reduced-order models in magnetodynamic problems," *IEEE Trans. Magn.*, vol. 52, no. 3, Mar. 2016, Art. no. 7204804.



DAN WANG received the B.S. degree in mechanical engineering from the Dalian University of Technology, Dalian, China, in 2013, and the Ph.D. degree in mechatronic engineering from Zhejiang University, Hangzhou, China, in 2019. He is currently a Lecturer with the College of Mechanical and Electrical Engineering, Nanjing University of Aeronautics and Astronautics, Nanjing, China. His current research interests include nonlinear control of smart-material-based actuators, multiphysics, and multiscale simulation of complicated mechatronic systems.



YAoyao WANG received the B.S. degree in mechanical engineering from Southeast University, Nanjing, China, in 2011, and the Ph.D. degree in mechatronic engineering from Zhejiang University, Hangzhou, China, in 2016. He is currently an Associate Professor with the College of Mechanical and Electrical Engineering, Nanjing University of Aeronautics and Astronautics, Nanjing. His current research interests include robust control and adaptive control of underwater vehicle-manipulator systems, design, and control of cable-driven manipulators.



YONGHUA LU received the M.S. and Ph.D. degrees in mechanical engineering from the Nanjing University of Aeronautics and Astronautics, Nanjing, China, in 2003 and 2005, respectively. He is currently a Professor with the College of Mechanical and Electrical Engineering, Nanjing University of Aeronautics and Astronautics. His current research interests include intelligent detection, sensors, and robotics.



BAI CHEN received the B.S. and Ph.D. degrees in mechanical engineering from Zhejiang University, Hangzhou, China, in 2000 and 2005, respectively. He is currently a Professor with the College of Mechanical and Electrical Engineering, Nanjing University of Aeronautics and Astronautics, Nanjing, China. His current research interests include design and control of surgical robots, cable-driven robots, and sperm-like swimming micro robots.



LINXIANG WANG received the Ph.D. degree in mechatronic and control engineering from Zhejiang University, Hangzhou, China, in 1999, with emphasis on computer simulation and visualization of fluid flow and mixing. He is currently a Professor with the School of Mechanical Engineering, Zhejiang University. His current research interests include mathematical modeling of smart composites, design, and optimize of fluid power systems.



HONGTAO WU received the B.S. degree in mechanical engineering from the Northeast Heavy Machinery Institute (the name was changed to Yanshan University, in 1997), Tsitsihar, China, in 1982, and the M.S. and Ph.D. degrees in mechanical engineering from Tianjin University, Tianjin, China, in 1985 and 1992, respectively. He has been a Professor with the Nanjing University of Aeronautics and Astronautics (NUAA), Nanjing, China, since 1998. He has presided over numerous national research projects of China. He teaches the courses Introduction to Robotics and Computational Multibody System Dynamics at NUAA. His current research interests include multibody system dynamics, robotics, parallel mechanisms, and punching machines.

• • •